Available online at www.sciencedirect.com
SCIENCE DIRECT®
International Journal of Heat and Mass Transfer 47 (2004) 2637–2651
International Journal of HEAT and MASS TRANSFER
www.elsevier.com/locate/ijhmt

Numerical modeling of pulse combustor tail pipe heat transfer

Sridhar Thyageswaran *

Department of Mechanical Engineering, Coimbatore Institute of Technology, Coimbatore 641014, India

Received 2 February 2003; received in revised form 4 December 2003

Abstract

Multi-dimensional simulations of turbulent flow in a pulse combustor tail pipe were performed using the methodology of computational fluid dynamics (CFD) analysis. The flow in a pulse combustor tail pipe is complicated by periodic reversals amid large rates of convective heat transfer from the walls. The performance and limitations of two conventional quasi-steady near-wall turbulence models in predicting the wall heat transfer are presented. Within the context of a CFD-methodology, a flow-based near-wall turbulence model is proposed. Its capability for predicting heat transfer under oscillatory flow conditions is discussed.

Keywords: Pulse combustion; Periodic flow; Turbulence modeling; CFD analysis; Convective heat transfer

1. Introduction

Pulse combustion is driven and sustained by resonant pressure waves. Fig. 1 is a sketch of a simple pulse combustor, hereafter referred to as P-C. At the beginning of each cycle, fuel and oxidant are admitted into the reaction chamber by the opening of the pressure-operated one-way valve. Upon ignition, a compression wave travels along the tail pipe and reflects off as an expansion wave from the open end. The expansion wave returns and reflects off the closed end of the reaction chamber as another expansion wave. This lowers the pressure in the reaction chamber causing the valve to open and admit fresh charge. Meanwhile, the expansion wave returns to the reaction chamber as a compression wave after reflection from the open end of the tail pipe. If the ignition of the fresh charge is synchronized with the return of the compression wave the cycle becomes self-sustaining, causing a periodically reversing oscillatory motion of the gases in the tail pipe.

For several applications, P-Cs offer distinct advantages over conventional combustion devices, the most notable of which is an observed increase in the heat transfer rate through the walls of the reaction chamber and tail pipe [1–3]. Higher wall heat transfer rates translate into reduced size and cost of pulse combustion devices used for heating applications. The oscillatory motion of the products of combustion during each cycle improves reactant mixing. This enhances combustion efficiency and reduces the excess air requirement, apart from reducing the formation of soot, un-burnt hydrocarbons and carbon monoxide. Higher heat transfer rates imply that P-Cs can be operated at relatively lower temperatures. This minimizes the formation of oxides of nitrogen. Low quality fuels can be used since the combustion process is improved in the presence of large oscillations. P-Cs have a few disadvantages that, fortunately, can be taken care of relatively easily. Mechanical vibration in the structural components due to flow-induced resonance is one main drawback. However, with improved isolation devices and physical design of the system, mechanical vibrations can be controlled.

In this paper, the focus is on the heat transfer between the products of combustion and the walls of the tail pipe. Tail pipe heat transfer directly impacts P-C performance and is important for heating applications

* Address: "Vasantham", 24 Central Excise Colony, P.N. Pudur, Coimbatore 641041, India. Tel.: +91-422-2436692.
E-mail address: sthyages@yahoo.co.in (S. Thyageswaran).

0017-9310/$ - see front matter © 2004 Elsevier Ltd. All rights reserved.
doi:10.1016/j.ijheatmasstransfer.2003.12.020

Nomenclature

A^+	Turbulence length scale damping factor
B	amplitude of velocity oscillations
f_τ	wall-function coefficient for shear stress
h	convective heat transfer coefficient
H	channel half-height
k	turbulence energy
l	turbulence length scale
Nu	Nusselt number
P	pressure
P_k	turbulence kinetic energy production $= \mu_t(\mathrm{d}U/\mathrm{d}y)^2$
Pr	Prandtl number
q''	heat flux
Re	Reynolds number
t	time
T	temperature, cycle time-period
u_*	characteristic velocity of the turbulent wall layer $= C_\mu^{1/4} k_{\max}^{1/2}$
u_τ	friction velocity $= (\tau_w/\rho)^{1/2}$
U	stream-wise fluid velocity
U_e	stream-wise fluid velocity external to the boundary layer
V	bulk fluid velocity
x	stream-wise coordinate
y	span-wise coordinate

Greek symbols

γ	amplitude parameter
ε	turbulence dissipation rate
μ	molecular fluid viscosity
μ_t	turbulence viscosity
ν	kinematic viscosity
ρ	fluid density
τ	shear stress, normalized time $= t/T$
ω	frequency of oscillation

Subscripts

a	amplitude
avg	average
D	hydraulic diameter
g	gas
m	mean
osc-max	maximum oscillation amplitude
q.s.	quasi-steady
rms	root mean square
w	evaluation at the wall

Superscripts

n	exponent
+	dimensionless turbulence scaling

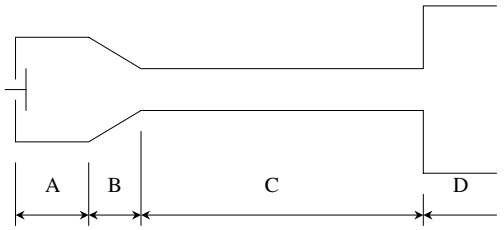

Fig. 1. Schematic diagram of a Helmholtz-type pulse combustor: A— combustion chamber, B—transition section, C—tail pipe, D—acoustic de-coupler.

of P-Cs. Despite the significant amount of research that has been performed on P-Cs to date most of it has been focused on the overall performance characteristics. Hence the basic mechanisms causing heat transfer enhancement under certain operating conditions are poorly understood. One reason for this is the complexity of the flow field in the tail pipe: it is multi-dimensional, periodic and highly turbulent. To complicate matters further, fluid properties are variable and energy addition occurs in time scales comparable to the fluid motion. Consequently, a model capable of predicting tail pipe heat transfer rates over a range of operating conditions is unavailable. Such a model is essential to pulse combustion system simulations that are being developed as practical design tools. Pulse combustion systems developed using trial-and-error approaches rely on data accumulated from experience gained by building and operating such devices. Such approaches cannot produce optimal designs. If the effects of the P-C operating parameters on the heat transfer can be found, these can be used to optimize the combustor performance over its complete operating range and help in P-C design.

2. Overview of tail pipe heat transfer research

Research contributions to pulse combustion and heat transfer under oscillatory flow conditions can be broadly classified into three categories.

2.1. Experimental studies

Martinelli et al. [4] were the first to observe an increase in the heat transfer rates for flows in the laminar regime. No significant increase in heat transfer rates was observed for turbulent flows. Using a gas-fired P-C, Hanby observed heat transfer enhancement of as much

as 240% over the corresponding steady flow [5]. Galitseyskiy and Ryzhov [6] report higher increases in heat transfer rates (as much as five times) in high frequency turbulent gas flows. However, other investigators report a decrease in heat transfer rates when compared to the corresponding steady flow values [7,8]. While in some instances the comparison with steady flow heat transfer rates was made using results obtained with the same arrangement that was used in the pulsing flow experiments, a more important explanation for the apparent inconsistency is that the operating parameters differed in all the studies. The results of several other investigations available in the literature are noteworthy [9–13]. In the early experimental studies the data were mostly obtained using mechanical pulsing devices at low frequencies. The more recent experiments have been performed at high frequencies under acoustic resonance conditions in a gas phase. A few empirical correlations for heat transfer in pulsing turbulent flows have also been proposed [14,15]. Such contributions provide useful tools for estimation of heat transfer rates, but do little by way of explaining the fundamental mechanisms responsible for heat transfer enhancement (or reduction) under pulsing flow conditions.

A detailed experimental study of pulse combustion was undertaken by Dec and Keller at Sandia National Laboratories [2]. The amplitude and frequency of the pulsations and the mean flow rate were varied systematically, in order to determine their influence on heat transfer. For a constant mean flow Reynolds number, Re_m, the Nusselt number, Nu, increased almost linearly with the pulsation frequency, ω, and amplitude. For a given ω and amplitude it was observed that Nu enhancement decreased with an increase in Re_m. The Sandia data has also been empirically correlated [16].

2.2. Analytical studies

Barnett and Vachon [17] analyzed the fully developed pulsating flow in a tube. They concluded that mean flow transients only increase heat transfer for low-frequency high-amplitude oscillations. At higher ω, the effect was to lower Nu below the corresponding steady flow value. Lee et al. [18] mathematically modeled a low-amplitude P-C using a Helmholtz resonator approach. One major simplification is to treat periodic flow as if it were steady at the instantaneous velocity. This "quasi-steady" approach implies that the flow attains equilibrium in a time scale that is much less than the cycle time period. This would only be possible if the frequency and amplitude of the imposed fluctuations are negligibly small. P-Cs operate in frequency and amplitude ranges that are far-removed from the quasi-steady limit. In spite of this, quasi-steady theory has found favor amongst many researchers, due to the lack of a suitable alternative approach.

The extension of quasi-steady theory to oscillating flows is best illustrated by the use of the steady flow Dittus–Boelter correlation [19]. Assuming the fluid velocity oscillates in a sinusoidal manner about a mean value V_m the correlation is re-written as

$$Nu_D(t) = CPr^n(D/v)^{0.8}(V_m|1 + B\cos\omega t|)^{0.8}. \quad (1)$$

The modulus insures that even when $B > 1$, Nu_D remains positive. Integration over a complete cycle yields the quasi-steady estimate, which is dependent only on the amplitude, B, and not the frequency, ω. The use of the Dittus–Boelter correlation imposes other restrictions on the use of Eq. (1) to study heat transfer in pulsing tail pipe flows. First, the pressure gradient cannot be considered negligible, since the velocity oscillations are driven by an oscillating pressure gradient. Second, the wall temperature must be independent of the stream-wise position, x. In practice, this condition is not fulfilled either. Clearly, the applicability of the quasi-steady theory for tail pipe heat transfer, in the manner des- cribed above, is highly questionable.

2.3. Numerical simulations

Many researchers have numerically simulated P-C operation. These include 1-D simulations of the flow in the reaction chamber and tail pipe, and combustion simulation, using the method of characteristics [20–23]. In this method, the equations are simplified by neglecting wall friction, wall heat flux and energy release during combustion. These assumptions are clearly very restrictive, since wall friction and heat transfer are enhanced by the presence of turbulence in the tail pipe flow, and change the entropy of the gas. Barr et al. studied P-C flows using a 1-D method that accounted for wall friction and heat transfer [24]. Their model requires data for the time-varying energy release and gas injection, which was supplied by experimental measurements. 1-D simulations are easy to implement in a numerical scheme, but by integrating the governing equations over the flow cross-section valuable information pertaining to variation of velocity and temperature across the flow is lost. The resulting solutions depend heavily on the wall flux information supplied. In many instances, unless this information is available a priori through experiments, it has to be supplied through steady flow correlations. Consequently the performance of the model becomes difficult to judge. In particular, if the aim is to understand the fundamental mechanisms that cause wall heat transfer enhancement in the presence of flow pulsations, 1-D models are inadequate. Numerical simulations of oscillatory flows have been performed by Stosic and Hanjalic [25], and Koehler et al. [26]; however, neither of these studies deals specifically with pulse combustion.

3. Objectives of the study

From the preceding section the need for a comprehensive heat transfer model that captures the essential physics of P-C tail pipe flow becomes clear. A powerful tool available for this purpose is multi-dimensional CFD analysis. The Sandia experiments [2] were chosen for the numerical simulations, with the following objectives:

1. Identify the mechanisms governing heat transfer in turbulent compressible pulsing flows, as exemplified by the P-C tail pipe flow.
2. Within the context of a multi-dimensional CFD methodology, develop a flow-based heat transfer model to properly represent the physics governing the P-C tail pipe flow.
3. Demonstrate the ability of the model to predict tail pipe heat transfer over a broad range of P-C operating conditions.

Predictions of tail pipe heat transfer were first obtained using a conventional two-equation turbulence model. The use of the conventional model revealed some of its inherent deficiencies for simulating P-C tail pipe flows. An alternative, quasi-steady near-wall turbulence model known as the boundary layer wall model [27] was implemented in the CFD analysis code. Based on its predictions, improvements to the boundary layer wall model were made to incorporate the effects of adverse and favorable pressure gradients on tail pipe heat transfer. The improved, flow-based model is referred to as the Unsteady Wall Layer Model. Tests over a range of typical P-C operating conditions indicate that the unsteady wall layer model is robust and is capable of capturing the effects of pulsation frequency, pulsation amplitude and Re_m on the tail pipe heat transfer.

4. Modeling and computation of the tail pipe flow

The mean fluid motion and heat transfer in the P-C tail pipe is governed by the time-averaged equations of continuity, momentum and energy. The time averaging poses a closure problem, and the additional terms must be suitably modeled [28]. For this purpose, two more equations representing the conservation of turbulence kinetic energy, k, and the turbulence dissipation rate, ε, are solved in their modeled forms. The k–ε model is the foundation on which the discussions in this paper are based.

The operating parameters of the baseline pulsing flow condition selected for detailed numerical study are summarized in Table 1. The combustion chamber P_{rms} amplitude of 7.4 kPa was sufficient to cause periodic flow reversals in the tail pipe. The tail pipe was 30 mm square in cross-section and terminated in a large volume acoustic de-coupler. For the steady, non-pulsing flow case the same pipe configuration was used. The difference in Re_m (3500 vs. 3750) is attributed to the temperature dependent μ and a marginally lesser mass flow rate. Measurements were made at a distance of $x = 540$ mm from the reaction chamber end. In the experiments, the tail pipe was surrounded by another co-axial square pipe and cooling air flowed in the annular space between the two pipes. In effect, the arrangement was a simple heat exchanger.

Table 1
Salient operating conditions for baseline flow

	Re_m	P_{rms}/kPa	ω/Hz	Length/mm
Baseline pulsing flow	3750	7.4	83	880
Non-pulsing flow	3500	*	*	880

The tail pipe flow is modeled as an unsteady turbulent flow in a 2-D channel, 30 mm high. The governing equations were solved using JCODE, a research CFD analysis program, based on the control-volume finite-difference technique [29]. The cyclic mass flow rate into the channel from the reaction chamber end was gradually adjusted to match the experimentally measured centerline velocity at the monitoring location. Since detailed measurements of the wall temperature, $T_w(x)$, were not available for the CFD analysis a simple mathematical model was developed to resolve this situation. The convective heat transfer coefficient, $h(x)$, obtained from the simulation of the channel flow was used in a simple 1-D model of the tail pipe heat exchanger. A differential model of heat exchange between the exhaust gas and cooling air through the intervening wall was developed. The model predicted the axial and temporal variation of the lumped gas and wall temperatures in the square tail pipe. The two sets of calculations proceeded simultaneously; the CFD simulation provided the wall temperature model with the requisite $h(x)$ values, and in return received information from the wall temperature model on the variation of $T_w(x)$. Upon convergence, the numerical results were monitored at $x = 540$ mm. Using the predicted h, the lumped gas temperature and T_w the heat flux, q''_w, and Nu at the walls of the square tail pipe are calculated. The results, analyzed in both time-resolved and cycle-averaged manner, for the various modeling approaches used are now presented.

4.1. Conventional modeling

The standard k–ε model relies on wall functions to avoid computations in the near-wall flow regions. In the wall-function approach, the turbulent boundary layer is delineated into two distinct zones. In each zone, it can be shown that the distributions of velocity and temperature follow a universal behavior under some crucial

assumptions. The algebraic relations expressing this universal behavior are called wall functions (WF). For the simulations the tail pipe region was divided into 88 cells along x, and 10 cells along y from the flow centerline. While the near-wall cell occupied nearly 32% of the channel half-height, the remaining 9 cells were equally sized. The reason for this non-uniformity is discussed later. Sensitivity studies insured that the results are independent of the grid cell size (in the bulk flow regions) and turbulence inlet boundary conditions. In Fig. 2, the predicted values of *Nu* using the WF approach are shown in a time-resolved manner along with the experimental measurements. For comparison, *Nu* for the baseline non-pulsing flow is also presented. It can be seen that under pulsing flow conditions the cycle-averaged *Nu* is higher than its corresponding steady flow value. However, while the experiments indicate a sharp increase in *Nu* during flow reversals, the numerical predictions show an opposite trend by decreasing to their lowest values during these times. The large size of the near-wall cell causes the predicted turbulence production at these nodes to follow the bulk flow behavior, directly impacting q''_w and hence *Nu*.

Denoting evaluation at the near-wall node by the subscript P, in the WF model the wall shear stress $\tau_w = f_\tau U_P/y_P$. If the near-wall node is inside the fully laminar region, $f_\tau = \mu$. Else, if the near-wall node is in the fully turbulent region of the boundary layer, $f_\tau = \rho C_\mu^{1/4} k_P^{1/2} \kappa y_P / \ln(E y_P^+)$. C_μ, κ and E are standard k–ε model constants. The dimensionless scaling of the y-coordinate is done as $y_P^+ = C_\mu^{1/4} k_P^{1/2} y_P/\nu$. The end result is that f_τ is discontinuous across the interface of the two regions, and results in a significant over-prediction of τ_w if the near-wall node is positioned inside the fully laminar region during the computations. A similar behavior is encountered in the prediction of q''_w. Hence, for all times during an oscillation cycle it must be insured that the near-wall nodes do not enter the fully laminar region. This explains the deliberate choice of the large-sized near-wall cells. As an immediate consequence of this, under pulsing conditions the near-wall flow cannot be adequately resolved for phase differences with the bulk flow. It is clear that WF k–ε modeling fails to adequately predict the time-resolved variations of velocity and heat transfer rate under typical P-C operating conditions. The assumption of an equilibrium behavior of the wall-layer flow, and an extension of a steady flow WF k–ε turbulence model to predict unsteady wall-bounded flows by simply including time derivatives in the governing equations assumes that the Reynolds stresses behave in a quasi-steady manner in spite of the imposed unsteadiness [30,31]. These assumptions fail when applied to P-C tail pipe flow.

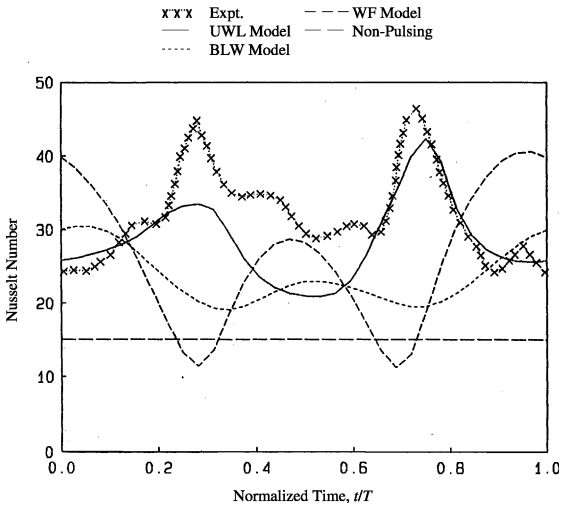

Fig. 2. Cyclic variation of Nusselt number at the monitoring location: baseline pulsing case.

4.2. Boundary layer wall model

The boundary layer wall model (BLWM) also adopts a two-tiered approach to resolve the turbulence flow field. In the outer bulk flow region the usual k–ε model is used, while in the near-wall boundary layer region a one-equation model of turbulence is used. The demarcation between the outer flow and the near-wall flow is chosen to occur at a selected value of y^+. The numerical solutions are merged at the chosen interface, insuring smooth transition of the flow variables between the two flow regions. In the BLWM, the model ε-equation is not solved below the selected y^+. Instead, l is prescribed using a formula that resembles the Van Driest damping function [32]. The model k-equation is solved all the way to the wall, however. There are some major advantages to using the BLWM for P-C tail pipe flows. First, a transport equation for ε is not solved in the near-wall region. An acceptable form of the modeled ε-equation is yet to be established and the resolution of ε near the wall requires an extremely fine mesh [33]. The BLWM imposes no such grid restrictions. Second, the model provides high resolution of the wall-layer flow compared to the WF approach. A third advantage is that, unlike the WF approach, the heat transfer predictions are independent of the near-wall cell size [27].

The governing equations are solved using one grid for both the near-wall layer and outer region of the flow. In the BLWM, the lower limit of the wall-layer region coincides with the thickness of the viscous sub-layer, $y^+ = 5$. Based on well-established measurements of turbulent boundary layer flow [34], the wall-layer is assumed to extend from $y^+ = 5$ to $y^+ = 50$. Using this scaling, the dimensional thickness of the near-wall flow is allowed to vary with x and t. A larger number of cells occupy the wall-layer region when the wall layer

thickens during the cycle, compared to intervals when the wall layer is relatively thinner. Below $y^+ = 50$,

$$l = \kappa y[1 - \exp(-y^+/A^+)], \quad A^+ = 26, \tag{2}$$

and $\varepsilon = C_\mu^{3/4} k^{3/2}/l$. Beyond $y^+ = 50$, which is the beginning of the fully turbulent region, the standard k–ε model equations are solved to yield the l-profiles. The wall-layer prescription of l is matched with the outer-layer length scale using function and derivative matching conditions at $y^+ = 50$. Since the BLWM allows positioning of the near-wall node within the viscous sublayer, τ_w and q''_w are computed directly using Newton's law and Fourier's law, respectively.

The predictions of the BLWM for the baseline pulsing flow were obtained using a mesh of 176 uniform cells along x and 15 non-uniform cells along y. The cell immediately adjacent to the wall was located at $y = 0.01H$. Simulation results with the near-wall cell located at $y = 0.00625H$ exhibited insensitivity to the size of the near-wall cell. Calculated profiles of U, during the first half of the oscillation cycle, are shown in Fig. 3 (profiles for the second half look similar). The velocity profiles are almost flat in the bulk flow regions, as would be expected for a turbulent flow. The centerline velocity starts from a maximum value of +95 m/s and reverses to a maximum value of −60 m/s. The centerline flow reversals occur at approximately $t/T = 0.26$ and $t/T = 0.67$ (T is the cycle time-period). It is clearly seen that the fluid near the wall reverses significantly earlier than the fluid near the center of the channel. The near-wall regions have lower momentum compared to the bulk flow, and hence they respond more rapidly to the oscillating pressure gradient. The WF model could not predict such a phase difference. From Fig. 3 it also appears as though nothing similar to the Richardson's

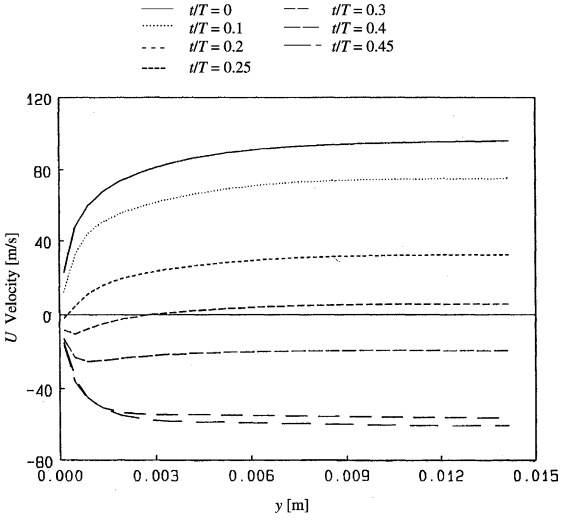

Fig. 3. Boundary layer wall model predictions of velocity profiles at the monitoring location: baseline pulsing case.

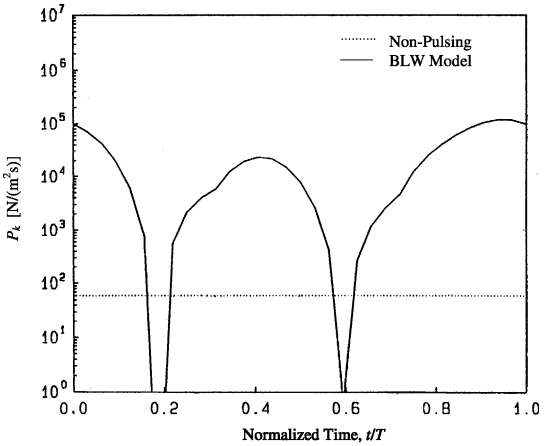

Fig. 4. Cyclic variation of turbulence energy generation at the wall: baseline pulsing case.

annular effect [35,36] exists for the case of turbulent oscillating flow in the P-C tail pipe. Similar observations were made during the experiments, from the measured U-profiles [37].

The time-resolved variation of Nu at $x = 540$ mm is shown along with the experimentally measured values in Fig. 2. For comparison, the Nu for non-pulsing flow and the WF predictions are also shown. The tendency of Nu to peak during times of zero crossing of the centerline velocity is not captured by the BLWM. Instead, roughly at these times Nu attains its minimum values. During the entire pulsation cycle the predicted Nu remains higher than the steady flow value of 15, a trend that is observed in the experiment. In contrast, the WF predictions of Nu become lower than the steady flow value for two very brief durations in a cycle. The enhancement in Nu due to flow pulsations can be explained by referring to Fig. 4 in which the cyclic variation of the dominant turbulence energy production term, P_k, is shown. Also shown is the corresponding value of P_k for the non-pulsing flow. In both cases, P_k was evaluated at the near-wall node on the $x = 540$ mm plane. At times of zero crossing of the velocity of the near-wall node (at $t/T = 0.19$ and 0.60), P_k is zero. At all other times during the cycle, P_k remains significantly higher than its value under steady flow conditions. This, in turn, leads to an increased u_* which is an indicator of the turbulence level in the wall layer. The magnitude of P_k under steady flow conditions is roughly 60 N/(m^{2}s), almost insignificant when compared with its values in the presence of large amplitude velocity oscillations.

4.3. The effect of pressure gradients

Before proceeding further, a small modification to the BLWM based on physical arguments is presented.

For the prescription of l in the BLWM, an empirical value of $A^+ = 26$ has been traditionally used for high Re flows [34]. The constant A^+ represents the effective thickness of the viscous sub-layer, and various researchers have used several alternative values [33,38,39]. In the present research a value of $A^+ = 52$ gave excellent predictions of q''_w and Nu for the non-pulsing flow. In the Sandia experiments, Re_m ranged from 3100 to 4750, which is extremely low for turbulent flow. Under non-pulsing flow conditions, $A^+ = 26$ over-predicted $Nu(x)$ at all stations by roughly 25%.

Under typical pulsing conditions, the fluid in the tail pipe experiences adverse and favorable pressure gradients twice during each cycle. The acoustic de-coupler end of the tail pipe is effectively an open end with pressure remaining equal to the atmospheric pressure. The combustion chamber pressure, on the other hand, varies in a sinusoidal manner during one pulsation cycle. Using $Q1$, $Q2$, $Q3$, and $Q4$ to denote the quarters of each cycle, during $Q1$ the fluid decelerates under an increasingly adverse pressure gradient until the velocity becomes zero. The flow reverses direction, and accelerates under a suddenly favorable pressure gradient during $Q2$. After attaining a peak velocity in the reversed direction the fluid decelerates once again, as the pressure gradient becomes adverse. The flow reverses direction at the end of $Q3$, and accelerates under a favorable pressure gradient in $Q4$. Therefore, while the velocity fluctuates at a frequency ω, the fluid resident in the tail pipe feels the effects of the imposed pressure gradient at twice the frequency, i.e. 2ω. It is well known that adverse pressure gradients enhance turbulence, whereas favorable pressure gradients suppress turbulence [35]. The response of the turbulent boundary layer to the imposed pressure gradients can be effectively modeled by allowing A^+ to vary during a cycle. So far, the treatment of A^+ can best be described as quasi-steady since its value remained constant during an entire cycle.

A simple way of enforcing this variation is through the use of Eq. (3):

$$A^+ = A^+_{\text{q.s.}}[1 + \gamma\cos(2\omega t)], \tag{3}$$

in which $A^+_{\text{q.s.}} = 52$ and $\gamma = 0.9$. As a consequence, with increasing adversity of the pressure gradient, $A^+ < A^+_{\text{q.s.}}$ whereas during times of favorable pressure gradient, $A^+ > A^+_{\text{q.s.}}$. Though the value of γ is arbitrarily assigned for now, the use of Eq. (3) helps shed valuable light on the heat transfer behavior in the tail pipe flow. The computational code was suitably modified, and the baseline pulsing flow case was simulated. The resulting prediction of $q''_w(t)$ at $x = 540$ mm is shown in Fig. 5. The prediction of the baseline BLWM is also shown, for comparison. The two peaks in the predicted q''_w coincide very nearly with the peaks in the experimental result. In the time interval between the first peak and the second,

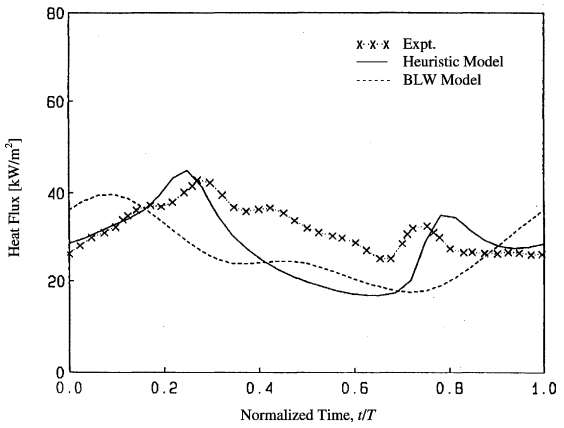

Fig. 5. Cyclic variation of wall heat flux at the monitoring location: baseline pulsing case.

the predicted q''_w remains lower in magnitude than the experimentally measured values. While the heuristic prescription of A^+ captures the twin peaks in the q''_w variation, such an approach is a crude expedient to model the effects of unsteady pressure gradients on the wall-layer turbulence. Heuristic prescriptions are tedious to devise and implement as the flow situation becomes complex and, more importantly, lack generality. The arbitrary specification of γ makes the approach appear problem-specific. A flow-based wall-layer turbulence model, capable of accommodating a broad range of changes under different flow situations, is highly desirable.

For the case of an ensemble-averaged oscillating turbulent flow in a pipe, in the central regions of the pipe, the fluid responds in a slug-like fashion to the imposed pressure gradient according to $\rho\partial U/\partial t = -\partial P/\partial x$. For sinusoidal oscillations, of the form $U = U_m(y) + U_a(y)\exp(i\omega t)$, the solution is given by $\omega\rho U_a = |\partial P/\partial x|$. Hence, even small amplitude velocity oscillations can cause the amplitude of the pressure gradient oscillations to be much larger than the mean pressure gradient, at large ω [40]. In the case of a P-C, the turbulent flow in the tail pipe is characterized by a time-varying pressure gradient whose effects on the turbulence must be modeled properly. Though several models have been developed to account for the effects of pressure gradients on turbulent boundary layers, in this paper the focus is on one-equation models. It has been suggested that the Van Driest prescription should not be used for flows with strong adverse pressure gradients [41]. Since y^+ is traditionally defined as $y^+ = u_\tau y/\nu$, the vanishing of τ_w at flow separation means the term $[1 - \exp(-y^+A^+)] = 0$, and hence l and μ_t will be inappropriately predicted as zero. In the BLWM, u_τ is replaced by u_* which is based on k. This way, even if $\tau_w \to 0$, l and μ_t in the wall layer remain non-zero.

Table 2
Various algebraic prescriptions for A^+

Prescription	Reference	Remarks
$A^+ = A^+_m[1 - 11.8p^+]^{1/2}$	[41]	$p^+ = (\nu/\rho u_\tau^3)(U_e \mathrm{d}U_e/\mathrm{d}x)$, steady flow
$A^+ = 25.0/(1 + 37.2p^+)$	[42]	$p^+ = (\nu/\rho u_\tau^3)(\mathrm{d}P/\mathrm{d}x)$, steady flow
$A^+ = A^+_m(1 - 25p^+ + 1540p^{+2} + \cdots)$	[40]	$A^+_m = 26$, pulsating flow

Three existing algebraic prescriptions for A^+ to model the effects of pressure gradients are summarized in Table 2. Each proposal has a serious shortcoming when applied to P-C flow or, in general, to flows with unsteady pressure gradients. Under certain operating conditions, large time-varying p^+ can cause the A^+ of each prescription to become negative or imaginary, which is clearly inappropriate. In all of these proposals, an adverse pressure gradient ($p^+ > 0$) causes a decrease in the value of A^+ whereas a favorable pressure gradient ($p^+ < 0$) causes an increase in the value of A^+. All proposals work best for small p^+ only. A key feature of the first two proposals for A^+ is that they were developed for steady flows. Although these models have been used for various turbulent flows, none of these have been applied specifically to P-C tail pipe flows. Attempts to simulate the base operating condition ($\omega = 83$ Hz) using all three prescriptions failed because of the prediction of a physically meaningless A^+.

4.4. The unsteady wall layer model

Consider an element of fluid adjacent to the wall, experiencing flow reversals under an imposed oscillatory pressure gradient. Four possible combinations of fluid velocity U and pressure distribution are possible, and these have been summarized in Table 3. Following convention, the entries in this table show both U and $\partial P/\partial x$ as positive when U is in the direction of increasing x and the pressure P increases with an increase of x. Under such conditions, for example, we have an adverse pressure gradient and $U\partial P/\partial x$ is positive. All four combinations can be identified with the conditions in the tail pipe during each quarter of the pulsation cycle. It is concluded that $U\partial P/\partial x > 0$ implies adverse pressure gradients, whereas $U\partial P/\partial x < 0$ implies favorable pressure gradients. It can be argued that A^+ should be allowed to depend on $U\partial P/\partial x$ (scaled in an appropriate manner) in order to model the effects of pressure gradients on turbulent oscillating flows with flow reversals. The formulation can be according to $A^+ = A^+(u^+p^+)$, where $u^+ = U_{avg}/u_*$ and $p^+ = (\mu_w/(\rho_w^2 u_*^3))(\partial P/\partial x)$. The term U_{avg} denotes a space-averaged U in the wall layer, *i.e.* $y^+ < 50$. There is another compelling reason for modeling the dependence of A^+ on $U\partial P/\partial x$. It will be recalled that it was necessary to allow A^+ to fluctuate at a frequency of 2ω, in order to qualitatively predict the peaks in $q''_w(t)$ during a pulsation cycle. Both U and $\partial P/\partial x$ oscillate in a sinusoidal manner at a frequency ω; hence $U\partial P/\partial x$ will oscillate at a frequency 2ω.

To formulate A^+ a few simple guidelines were used, and the following expression is proposed:

$$\begin{aligned} &A^+ = [2\exp(-a)/(\exp(-a) + \exp(a))]A^+_{q.s.}, \\ &a = 6.0u^+p^+, \text{if } u^+p^+ > 0, \\ &a = 1.7u^+p^+, \text{if } u^+p^+ < 0. \end{aligned} \tag{4}$$

The exponential functions prevent A^+ from becoming negative during any part of the calculations. It will be recalled that $|\partial P/\partial x|$ is directly proportional to ω. Under very low ω, $|\partial P/\partial x|$ becomes small and its effect on the near-wall turbulence is expected to be insignificant. Hence, as $p^+ \to 0$, $a \to 0$, and A^+ then equals its quasi-steady value of 52. It will be noted that $a = 0$ when $u^+ = 0$, not just when $p^+ = 0$. However, $u^+ = 0$ only twice during a pulsation cycle when U_{avg} becomes zero. Under these flow conditions the effect of the pressure gradient on the turbulent flow is expected to be immaterial. Finally, it will be observed that when $a > 0$ (adverse $\partial P/\partial x$) the expression predicts $A^+ < 52$, and when $a < 0$ (favorable $\partial P/\partial x$) the expression predicts $A^+ > 52$.

When the proposed variation of A^+ (Eq. (4)) was implemented in the BLWM, it was observed that whereas the predicted Nu showed two peaks during its

Table 3
Velocity and pressure gradients in the pulse combustor tail pipe

	Quarter of the pulsation cycle			
	I	II	III	IV
Velocity	$U > 0$	$U < 0$	$U < 0$	$U > 0$
Pressure gradient	$\partial P/\partial x > 0$	$\partial P/\partial x > 0$	$\partial P/\partial x < 0$	$\partial P/\partial x < 0$
$U\partial P/\partial x$	> 0	< 0	> 0	< 0
Flow conditions	Adverse	Favorable	Adverse	Favorable

variation in one cycle both these peaks occurred significantly earlier in time than the peaks obtained in the experiments. The peaks occurred at $t/T = 0.18$ and 0.59 (compared to $t/T = 0.28$ and 0.72, respectively, in the experiments). In its present form, therefore, the model is still incapable of predicting the correct phase behavior of the wall heat transfer. For unsteady turbulent flows in which the pressure gradient changes rapidly, the assumption of an inner-region quasi-steadiness implied by Eq. (4) is inappropriate. The instantaneous change of A^+ with u^+p^+ requires that the conditions within the inner regions attain equilibrium in a time-scale that is much smaller than the time-period of the imposed unsteadiness. This is only possible if the changes in $\partial P/\partial x$ occur at an extremely low ω. If $\partial P/\partial x$ changes rapidly in time, the response of the sub-layer lags changes in $\partial P/\partial x$. A similar argument holds for the case of a steady turbulent boundary layer in which $\partial P/\partial x$ changes rapidly along x. A popular approach to model the delayed response of the sub-layer, to rapid changes in p^+ is through the use of lag equations of the form [39,42].

$$\mathrm{d}A^+_{\mathrm{eff}}/\mathrm{d}x^+ = C_L(A^+ - A^+_{\mathrm{eff}}). \tag{5}$$

In Eq. (5), A^+_{eff} is the "effective" value corresponding to the quasi-steady estimate of A^+, C_L is a modeling constant, and $x^+ = u_\tau x/\nu$. A rate equation similar to Eq. (5),

$$\mathrm{d}(\partial P/\partial x)_{\mathrm{eff}}/\mathrm{d}(tu_*^2/\nu) = C_L[(\partial P/\partial x) - (\partial P/\partial x)_{\mathrm{eff}}], \tag{6}$$

was used in the past to predict τ_w in turbulent, pulsating pipe flow [40]. In this case too, the reasoning used was that the sub-layer would not respond instantaneously to rapid changes in p^+. Hence, additional equations to introduce lag effects appear necessary.

Different operating conditions were simulated using the prescription for A^+ given in Eq. (4). The cases selected were at $\omega = 67$, 74, 83 and 101 Hz, and had been investigated experimentally by varying the length of the P-C tail pipe [2]. When plotted against normalized cycle time, the peaks in Nu occur at almost identical instances during the cycle, $t/T = 0.2$ and 0.6, for all four cases. The similarity among the predicted phase behavior and the experimentally observed phase behavior of q''_w, for all the four pulsation frequencies implies that a lag equation of the form

$$\mathrm{d}A^+_{\mathrm{eff}}/\mathrm{d}\tau = C_L(A^+ - A^+_{\mathrm{eff}}) \tag{7}$$

could be used to model the first-order response of the wall-layer turbulent boundary layer in the P-C tail pipe to an imposed unsteady pressure gradient. The variable $\tau = t/T$, and after several trials a value of $C_L = 70$ was chosen. Eqs. (4) and (7) taken together complete the prescription for the unsteady wall layer model (UWLM).

5. Results and discussion

The base operating condition was simulated using different grid arrangements to insure that the results are grid-independent. All the results discussed in this section are based on a mesh consisting of 176 cells in the x-direction and 15 cells in the y-direction, with a near-wall resolution of $0.01H$. Fig. 6 shows the temporal variation of q''_w at the monitoring location along with the experimentally measured values. Also shown are the variations of $q''_w(t)$ obtained using the WF model and the baseline BLWM. It can be seen that with the UWLM the peaks in q''_w, which occur approximately during the times of zero crossing of the centerline velocity, are predicted properly. Both the magnitude and the phase-position of the peaks in q''_w are captured well. The agreement between the numerical prediction and the measurements of q''_w deteriorates during the time interval $0.3 \leqslant t/T \leqslant 0.67$, shortly after the first zero crossing of the fluid velocity. During this interval, the measured values remain higher than the numerical predictions.

The numerical prediction of the cyclic variation of Nu in the 2-D channel using the UWLM is plotted in Fig. 2 along with the experimentally obtained variation. The variations of $Nu(t)$ predicted by the WF model and the baseline BLWM are also shown. In a manner similar to q''_w, the phase variation of Nu is predicted very well. Peaks occur in the predictions at instances that are almost synchronous with the experimental measurements, roughly during the times of zero crossing of the fluid velocity. The magnitude of Nu is predicted reasonably well during the quarters of the cycle preceding the first reversal of the gas velocity and following the second reversal of the gas velocity. In the intervening period, the predicted Nu does not compare favorably with the experimental values, consistent with $q''_w(t)$ behavior during this interval (see Fig. 6).

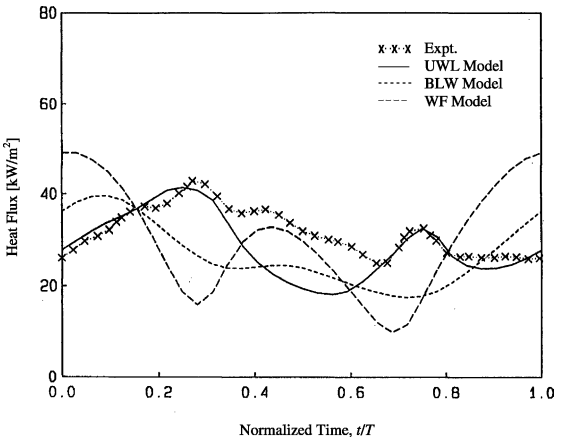

Fig. 6. Cyclic variation of wall heat flux at the monitoring location: baseline pulsing case.

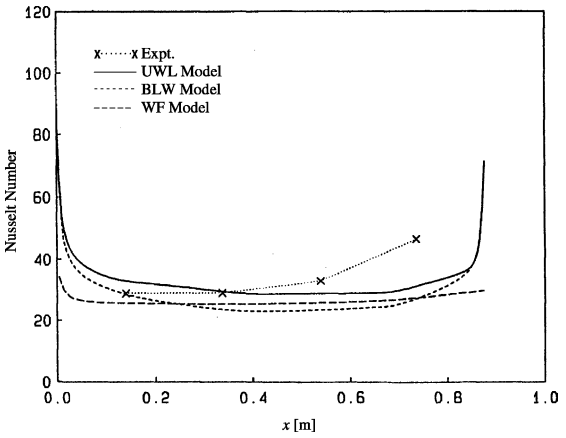

Fig. 7. Axial variation of cycle-averaged Nusselt number: baseline pulsing case.

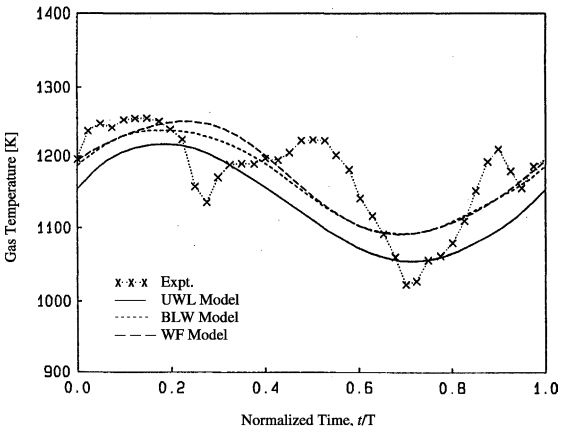

Fig. 8. Cyclic variation of gas temperature at the monitoring location: baseline pulsing case.

The cycle-averaged $Nu(x)$ variation is shown in Fig. 7. The results of the WF model and the baseline BLWM are also shown. The agreement between the predictions of the UWLM and the measured values is good, except at the last station, $x = 740$ mm. The sharp variation in Nu observed near the reaction chamber end of the tail pipe (and, to a lesser extent, at the acoustic de-coupler end) indicates the presence of hydrodynamic and thermal entrance regions. Closer to the acoustic de-coupler end, the measurements indicate large rates of q''_w than those predicted by the numerical model. The reason could be that regions of separated flow may exist near the sharp-edged corners of the tail pipe and de-coupler junction. However, no detailed measurements were made to confirm the existence of separated flow near this end of the tail pipe [2]. In order to verify the speculation it is necessary to include the de-coupler in the calculation domain at the expense of a significant increase in the number of grid points. For this reason, and in accordance with the other objectives of this study, such calculations were not made.

The time-resolved variation of the gas bulk temperature, T_g is compared with the measured variation, in Fig. 8. The predicted temperature variation is nearly sinusoidal, similar to the predictions of the WF model and baseline BLWM. Unlike the experimental variation, the predicted T_g does not undergo a reduction during times of zero crossing of the centerline velocity. All the calculations predict a cyclic variation of T_g consistent with the back-and-forth advection of enthalpy. While it could be argued that the sudden decrease in T_g is due to an increased q''_w during flow reversal, the subsequent increase in T_g as seen in the measured data is not readily explainable. Since the experimental measurements of T_g were confined to the transverse mid-plane ($z = 0$) of the square cross-section tail pipe, it has been suggested that this increase could be due to transverse flows in the tail pipe during flow reversal [43]. With the use of a 2-D channel as the calculation domain, instead of the actual tail pipe with its square cross-section, it is impossible to evaluate this possibility. The axial variation of the cycle-averaged gas temperature, $T_g(x)$, predicted by the UWLM is shown in Fig. 9 along with the measurements and the results of the WF model and the baseline BLWM. It is apparent that the agreement between the predictions and the measurements is good for most of the entire length of the tail pipe. Near the de-coupler end, however, the calculated T_g tends to be higher than the measurements.

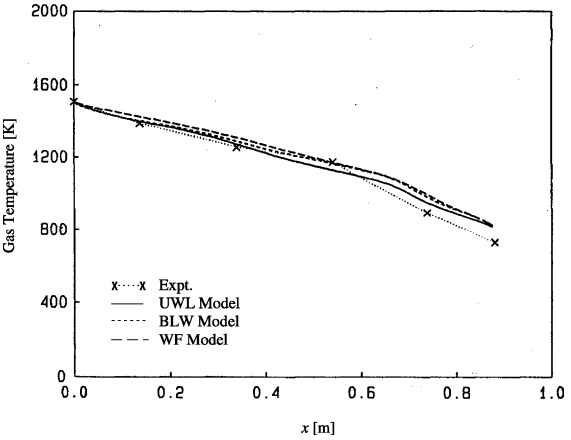

Fig. 9. Axial variation of cycle-averaged gas temperature: baseline pulsing case.

5.1. The effect of pulsation frequency

For studying the effects of pulsation frequency on the heat transfer, the length of the tail pipe was varied to alter the natural resonance frequency of the P-C [2]. In

addition, controlling the mixing rate of the reactants and the chemical reaction rate also enabled the frequency and amplitude of pulsations to be varied. In this manner, pulsation frequencies from 54 to 101 Hz were studied. Stable operation of the P-C was difficult below 67 Hz, hence swirl-injection of the reactants was resorted to for $\omega = 54$, 59 and 65 Hz. At the remaining frequencies of 67, 74, 83 and 101 Hz, axial injection was used. With a 2-D model of the tail pipe region numerical studies of the operation with swirl-injection could not be made. The flow cases with axial-injection were simulated numerically and the results were compared with the experimental measurements.

In the experiments, ω did not vary independently of the other operating parameters. Most notably, changes in the length of the tail pipe caused a variation in the inlet and exit temperatures of the exhaust gas. This caused a variation in the thermal properties of the gas resident in the tail pipe, affecting heat transfer in a complicated manner. The *r.m.s.* values of the combustion chamber pressure oscillations varied with changes in the tail pipe length, as well. Therefore, isolation of the effect of ω on the P-C tail pipe heat transfer is, strictly speaking, impossible. However, certain trends in the tail pipe heat transfer emerge when *Nu* is plotted against ω.

In Fig. 10, the variation of the cycle-averaged *Nu* averaged over the entire length of the tail pipe is shown for the four frequencies of pulsation that were simulated. Also shown are the spatially averaged values of *Nu* obtained in the experiments using standard heat exchanger log-mean temperature difference (LMTD) calculations [2]. It can be seen that both the numerical predictions and the experimental results indicate that the spatially averaged *Nu* increases with ω. The predictions suggest that at lower frequencies the Nusselt number increases sharply, but levels off as ω increases beyond 83 Hz. A similar trend is observed in the experimental

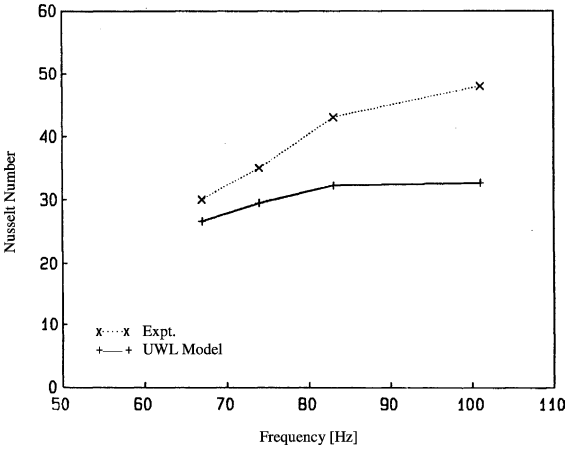

Fig. 10. Cycle- and space-averaged Nusselt numbers: effect of pulsation frequency.

results. The numerical simulations predict spatially averaged *Nu* values that are smaller than their corresponding experimental values, for each of the four operating frequencies that were considered. Little attention should be paid to this discrepancy, due to the substantial difference in the calculation approaches used. The experiments used a standard LMTD relation based on (a) an adiabatic heat exchanger, and (b) fluids of constant specific heat. Both these assumptions are violated since the outside surface of the annular tail pipe assembly was exposed to ambient air, and the exhaust gas temperature undergoes a 500 K drop from inlet to exit. The numerical calculations, however, provide detailed axial resolution of the cycle-averaged *Nu* without any of the simplifying assumptions used in the experiments.

The effects of pulsation frequency on the tail pipe heat transfer can be traced back to the effects of ω on the amplitude of the imposed pressure gradient in the tail pipe. As has been shown in Section 4.3, if ρ and U_a are considered invariant, $|\partial P/\partial x|$ is directly proportional to ω. It is therefore expected that an increase in pulsation frequency and pressure gradient amplitude will influence the turbulence in the tail pipe, which we model through the use of the pressure gradient parameter, u^+p^+.

5.2. The effect of pulsation amplitude

For each resonance frequency that was studied in the experiments, the energy release from combustion was timed to yield the maximum pulsation amplitude. The combustion chamber pressure, P_{rms} was used as a measure of the pulsation amplitude. In order to study the effects of pulsation amplitude on tail pipe heat transfer at each ω, the pulsation amplitudes were decreased from their maximum values by the addition of varying amounts of nitrogen. The effects of pulsation amplitude at $\omega < 67$ Hz were studied with swirl-injection of the reactants. The remaining cases at 67, 74, and 101 Hz were studied with axial injection. Unlike swirl-injection, which allowed the P-C to be operated stably over a range of pulsation amplitudes, the axial-injection cases were limited to a relatively narrow range of pulsation amplitudes. In addition, for the axial-injection cases the range of pulsation amplitudes over which measurements were possible narrowed as ω increased from 67 to 101 Hz [2].

In the experiments, for a given ω, an increase in the combustion chamber P_{rms} coincided with an increase in the velocity oscillation amplitude, $U_{osc\text{-}max}$ at the monitored location. The time-averaged mean velocity, U_m showed a tendency to increase as P_{rms} decreases for a given ω. The increase in U_m is due to the detuning of the energy release rate with an increase in the mass flow rate of nitrogen. Fig. 11 shows the effect of combustion chamber P_{rms} on the tail pipe heat transfer, for the

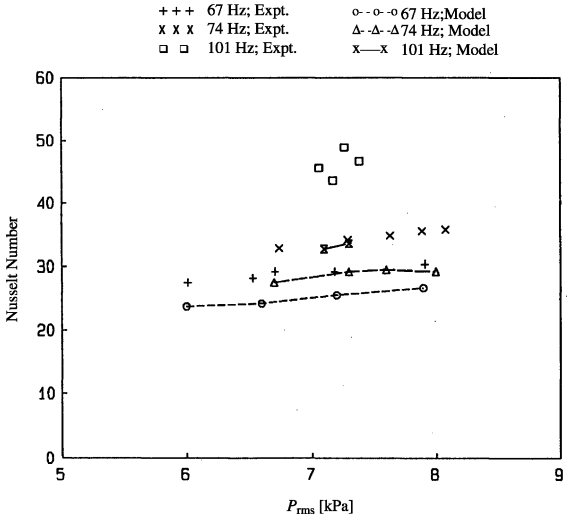

Fig. 11. Effect of pulsation amplitude on cycle- and space-averaged Nusselt number.

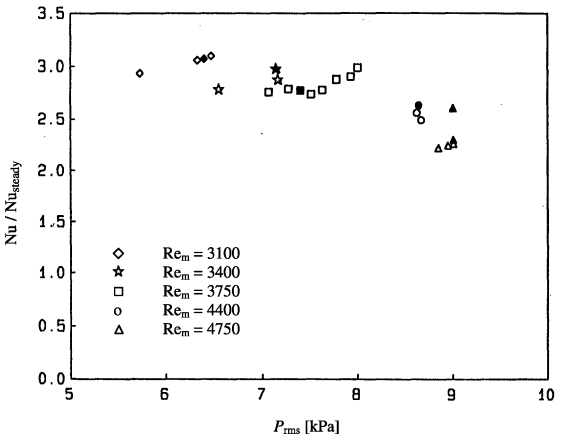

Fig. 12. Cycle- and space-averaged Nusselt numbers: effect of mean flow Reynolds number. The filled symbols represent predictions of the unsteady wall layer model.

pulsation frequencies that were studied using axial injection. Both the measured and the predicted values of *Nu* are shown. The numerical simulations were restricted to four pulsation amplitudes at 67 and 74 Hz, and only two closely-spaced pulsation amplitudes at 101 Hz. Enough data was not available to study the effects of pulsation amplitude at $\omega = 83$ Hz.

From Fig. 11 it can be seen that for a given pulsation amplitude, *Nu* increases with ω. This trend is observed in both the experimental and the numerical results, and is consistent with the trend in Fig. 10. In addition, for a given ω, *Nu* increases with pulsation amplitude. Both the measurements and the numerical predictions support this conclusion. Except at 74 Hz, for which the *Nu* shows a slight decrease when P_{rms} increases from 7.6 to 8.0 kPa, for all other frequencies there is a distinct increase in *Nu* with pulsation amplitude. As the pulsation amplitude increases at a particular ω, the magnitude of the velocity oscillations in the tail pipe increases, causing an increase in the turbulent heat transfer at the wall.

5.3. The effect of mean flow rate

By varying the mean mass flow rate of reactants supplied to the combustor, and the amount of nitrogen added to the products of combustion, the effects of Re_m on the tail pipe heat transfer enhancement were studied [2]. An increase in the mean mass flow rate of the reactants implies an increase in the thermal energy release, and a corresponding increase in the combustion chamber P_{rms}. A range of Re_m varying from 3100 to 4750 were studied experimentally, using a tail pipe whose length was constant. Despite the inability to vary the mean mass flow rate independently of ω and P_{rms} the experimental results indicate a definitive trend in the heat transfer enhancement with Re_m.

Fig. 12 is a reproduction of a plot published in the experiments showing the effects of Re_m on *Nu*, relative to steady flow at the same Re_m. Observations were made at $Re_m = 3100$, 3450, 3750, 4400 and 4750. The abscissa of Fig. 12 is the combustion chamber P_{rms} which varied from one case to the next, while the ordinate is the ratio expressing the Nusselt number enhancement. The time and space-averaged *Nu* during pulsing flow was obtained using LMTD heat exchanger calculations at each operating condition, as mentioned earlier. The corresponding steady flow *Nu* was obtained using the Dittus–Boelter correlation [19]. When plotted in this manner, it is observed that the heat transfer enhancement decreases with an increase in Re_m. While the data points for $Re_m = 3100$, 3450 and 3750 lie closely bunched around the factor 2.75, there is a noticeable decline in the enhancement at $Re_m = 4400$ and 4750.

Based on the experimental results shown in Figs. 10 and 11, where it was observed that the *Nu* enhancement increases with ω and pulsation amplitude, it was concluded that the decrease in *Nu* enhancement with an increase in Re_m is a definitive trend. In order to evaluate this trend, the UWLM was used to simulate some of the cases studied in the experiments. The simulations yielded one data point for each Re_m and the predictions are shown in Fig. 12 using filled symbols. It was observed that as the value of Re_m increases, the ratio $U_{osc\text{-}max}/U_m$ decreases. The decrease in the velocity amplitude ratio occurs simultaneously as the ratio Nu/Nu_{steady} decreases. This dependence of the *Nu* enhancement on the parameter $U_{osc\text{-}max}/U_m$ can be explained in the following manner.

For turbulent flow in a duct, the major contribution to the generation of turbulence energy in the near-wall region comes from the wall shear stresses acting on the

mean velocity gradient in the flow. In the P-C tail pipe, the generation of turbulence energy under pulsing flow conditions is expected to be significantly larger than the generation of turbulence energy under non-pulsing flow conditions (see Fig. 4). The increase is attributable to an increase in the velocity gradient (and therefore τ_w) caused by the imposed velocity oscillations. Consider two hypothetical cases of gas flow in a duct. In the first case, the steady flow Re is extremely small (U_m is nearly zero). Under these conditions, the heat transfer to the walls of the duct is also expected to be extremely small (Nu_{steady} is nearly zero). At this stage, the gases in the duct are subjected to a large amplitude oscillation, $U_{osc\text{-}max}$. As a result, the heat transfer will increase because of an increase in turbulence within the duct, leading to essentially a very large amount of heat transfer enhancement. In other words, the ratios $U_{osc\text{-}max}/U_m$ and Nu/Nu_{steady} will be large numbers. In comparison, if for the second case the Reynolds number under non-pulsing flow were quite large to begin with, the steady-state heat transfer to the walls of the duct would be substantial as well. The imposition of a velocity oscillation identical to the first case will result in relatively small values for the ratios $U_{osc\text{-}max}/U_m$ and Nu/Nu_{steady}. Hence the ratio $U_{osc\text{-}max}/U_m$ plays an important role in determining the heat transfer enhancement. For the five cases that were used to study the effects of Re_m, the ratio $U_{osc\text{-}max}/U_m$ monotonically decreases, causing a decline in the heat transfer enhancement with an increase in Re_m.

6. Conclusions

It was demonstrated that the use of the conventional wall-function (WF) k–ε model is inadequate to predict the magnitude and phase of the time-resolved heat transfer to the walls of the tail pipe under pulsing flow conditions. WF modeling could not adequately resolve the phase difference between the near-wall and bulk flow in the presence of flow pulsations. Attempts to resolve the near-wall flow, with more computational cells in the oscillatory boundary layer, caused the near-wall nodes to enter the fully viscous domain. This, in turn, causes deterioration in the results as WF predictions of τ_w and q''_w depend heavily on the local y^+-scaling of the near-wall nodes. The influence of the positioning of the near-wall nodes on the results demands some a priori knowledge of the flow field on the part of the user. The limitations of the WF model in providing a detailed resolution of the near-wall flow field directly impacts the predictions of q''_w which is governed primarily by the dynamics of the near-wall flow.

An alternative quasi-steady near-wall turbulence model demonstrated superior capabilities in resolving the near-wall flow. The boundary layer wall model (BLWM) uses an algebraic prescription for the near-wall l, and eliminates the computational burden of solving a transport equation for ε with several nodes in the near-wall region. Using this model it is possible to position nodes very close to the wall and obtain a detailed resolution of the phase differences between the near-wall and bulk flow velocities under pulsing flow conditions. Unlike the WF model, no ad hoc restrictions are imposed on ε at the near-wall nodes. This allows the near-wall nodes to adjust themselves to the time-varying conditions of the wall-layer flow during the pulsing operation of the combustor. However, similar to the WF results, the magnitude and phase of the time-resolved q''_w predictions are poor during pulsing operation of the combustor. In the presence of flow pulsations, the time-resolved Nu prediction of the quasi-steady BLWM shows a distinct increase over its steady flow value. This is due to an increased production of k, driven by an increase in the mean flow strain rate in the presence of large amplitude velocity oscillations.

Significant improvements in the phase predictions of the time-resolved q''_w were noted when the BLWM was modified to accommodate a time-varying A^+ in the prescription for l. It was argued that the notion of adverse or favorable pressure gradient on the near-wall flow could be addressed by the sign of the term $U\partial P/\partial x$. A dimensionless prescription for A^+ was formulated as $A^+ = A^+(u^+p^+)$. The Unsteady Wall Layer Model (UWLM), which uses a flow-based prescription for A^+ also assumes a delayed response of the near-wall layer turbulence to the rapidly fluctuating pressure gradient. The resulting predictions of wall heat transfer were found to be in good agreement with the measurements for the base operating condition. The time-resolved variation of the gas temperature showed a sinusoidal behavior, indicative of the back-and-forth advection of enthalpy. The sudden decrease in the gas temperature during flow reversals, as observed in the experiments, was not captured. The UWLM was used to study the effects of pulsation frequency, pulsation amplitude and mean flow Reynolds number on heat transfer enhancement under pulsing flow conditions. Several operating conditions from the experiments, encompassing a range of ω from 67 to 101 Hz, pulsation amplitudes (quantified by the combustion chamber P_{rms}) from 6.0 to 9.0 kPa, and Re_m from 3100 to 4750, were simulated. Even though the operating parameters could not be varied with complete independence, the proposed model captures the observed trends in the heat transfer enhancement due to variations in ω, pulsation amplitude and Re_m.

7. Summary

A computational turbulence model has been developed for the prediction of heat transfer to the walls of a

P-C tail pipe. The primary objective was to fill a void that currently exists in the field of P-C heat transfer modeling, by developing a CFD-based model that can be used as a practical design tool for P-C system simulations. By simulating several flow cases from the experiments [2], it was observed that the proposed model correctly captures the trends in heat transfer enhancement due to an increase of pulsation frequency, pulsation amplitude and mean flow Reynolds number. All the models discussed in this paper, however, failed in predicting the sudden decrease (and subsequent increase) in the gas temperature observed in the experiments during the times of flow reversal. To evaluate whether the gas temperature behavior during flow reversals is influenced by transverse flows as has been suggested [43], a 3-D model of the square cross-section tail pipe domain must be used. Full 3-D simulations could also help in further evaluation of the proposed Unsteady Wall Layer Model, using experimental cases that involved swirl injection of reactants.

References

[1] B.T. Zinn, Pulse combustion, The World and I, 1991, pp. 304–311.

[2] J.E. Dec, J.O. Keller, Pulse combustor tail pipe heat transfer dependence on frequency, amplitude, and mean flow rate, Combust. Flame 77 (1989) 359–374.

[3] G.K. Hargrave, J.K. Kilham, A. Williams, Operating characteristics and convective heat transfer of a natural gas-fired pulsating combustor, J. Inst. Energy 59 (439) (1986) 63–69.

[4] R.C. Martinelli, L.M.K. Boelter, E.B. Weinberg, S. Yakahi, Heat transfer to a fluid flowing periodically at low frequencies in a vertical tube, ASME Trans. 65 (1943) 789–798.

[5] V.I. Hanby, Convective heat transfer in a gas-fired pulsating combustor, ASME J. Eng. Power 91 (1969) 48–52.

[6] B.M. Galitseyskiy, Y.A. Rhyzov, Heat transfer in turbulent gas flows in the case of high-frequency pressure fluctuations, Heat Transfer—Sov. Res. 9 (4) (1977) 178–183.

[7] A.A. Al-Haddad, G.A. Coulman, Experimental and theoretical study of heat transfer in pulse-combustion heaters, Proceedings Volume I: Symposium on Pulse Combustion Applications, GRI-82/0009.2, Atlanta, GA, 1982.

[8] N.S. Liao, C.C. Wang, J.T. Hong, An investigation of heat transfer in pulsating turbulent pipe flow, ASME 23rd National Heat Transfer Conference, August 4–7, Denver, CO, in: F.A. Kulacki, R.D. Boyd (Eds.), Fundamentals of Forced and Mixed Convection, HTD-vol. 42, 1985, pp. 53–60.

[9] F.B. West, A.T. Taylor, The effect of pulsations on heat transfer to turbulent flow of water inside tubes, Chem. Eng. Prog. 48 (1) (1952) 39–43.

[10] R. Lemlich, Vibration and pulsation boost heat transfer, Chem. Eng. 68 (10) (1961) 171.

[11] M.H.I. Baird, G.J. Duncan, J.I. Smith, J. Taylor, Heat transfer in pulsed turbulent flow, Chem. Eng. Sci. 21 (1966) 197–199.

[12] R.H. Keil, M.H.I. Baird, Enhancement of heat transfer by flow pulsation, Indust. Eng. Chem.: Process Des. Develop. 10 (4) (1971) 473–478.

[13] S.K. Gupta, R.D. Patel, R.C. Ackerberg, Wall heat and mass transfer in pulsatile flow, Chem. Eng. Sci. 37 (12) (1982) 1727–1739.

[14] A.A. Al-Haddad, N. Al-Binally, Prediction of heat transfer coefficient in pulsating flow, Int. J. Heat Fluid Flow 10 (2) (1989) 131–133.

[15] A.A. Kornhauser, J.L. Smith, Heat transfer with oscillating pressure and oscillating flow, Proceedings of the 24th Intersociety Energy Conversion Engineering Conference, vol. 5, Washington D.C., August 6–11, 1989, pp. 2347–2353.

[16] V.S. Arpaci, J.E. Dec, J.O. Keller, Heat transfer in pulse combustor tailpipes, Combust. Sci. Technol. 94 (1993) 131–146.

[17] D.O. Barnett, R.I. Vachon, An analysis of convective heat transfer for pulsating flow in a tube, in: Proceedings of the Fourth International Conference, Paris-Versailles, France, Heat Transfer 1970 3 (1970).

[18] J.H. Lee, B. Dhar, W. Soedel, Mathematical model of low amplitude pulse combustion systems using a Helmholtz resonator-type approach, J. Sound Vib. 98 (3) (1985) 379–401.

[19] F.P. Incropera, D.P. DeWitt, Fundamentals of heat and mass transfer, third ed., John Wiley and Sons, New York, NY, 1990.

[20] L.D. Winiarski, A method for calculating non-steady compressible flow in a propulsive duct, Ph.D. Thesis, Oregon State University, Corvallis, OR, 1972.

[21] J.G. Craigen, Mathematical model of a pulsating combustor, Ph.D. Thesis, The University of Durham, United Kingdom, 1975.

[22] B. Ponizy, S. Wojcicki, On modeling of pulse combustors, Twentieth Symposium (International) on Combustion, The Combustion Institute, 1984, p. 2019.

[23] Y. Tsujimoto, N. Machii, Numerical analysis of a pulse combustor, Twenty-first Symposium (International) on Combustion, The Combustion Institute, 1986, p. 539.

[24] P.K. Barr, H.A. Dwyer, T.T. Bramlette, A one-dimensional model of a pulse combustor, Combust. Sci. Technol. 58 (1988) 315.

[25] N. Stosic, K. Hanjalic, Numerical study of unsteady convective heat transfer in pulsating duct flows, in: U. Grigull, E. Hahne, K. Stephan, J. Straub (Eds.), Heat Transfer, vol. 3, Hemisphere Publishing Corporation, New York, 1982.

[26] W.J. Koehler, S.V. Patankar, W.E. Ibele, Numerical prediction of turbulent oscillating flow in a circular pipe, Proceedings of the 25th Intersociety Energy Conversion Engineering Conference, vol. 5, Reno, NV, Aug 12–17, 1990, pp. 398–406.

[27] M.J. Jennings, Modeling of combustion chamber convective heat transfer for internal combustion engines, Ph.D. Thesis, Illinois Institute of Technology, Chicago, IL, 1991.

[28] H. Tennekes, J.L. Lumley, A first course in turbulence, The MIT Press, Cambridge, MA, 1972.

[29] A.D. Gosman, R.J.R. Johns, A simple method for generating curvilinear orthogonal grids for numerical fluid

mechanics calculations, Report Number FS/79/23, Department of Mechanical Engineering, Imperial College, London, United Kingdom, 1979.
[30] J. Cousteix, R. Houdeville, J. Javelle, Response of a turbulent boundary layer to a pulsation of the external flow with and without adverse pressure gradient, in: R. Michel, J. Cousteix, R. Houdeville (Eds.), Unsteady Turbulent Shear Flows, Springer-Verlag, Berlin, Germany, 1981.
[31] R.R. Mankbadi, A. Mobark, Quasi-steady turbulence modeling of unsteady flows, Int. J. Heat Fluid Flow 12 (2) (1991) 122–129.
[32] E.R. Van Driest, On turbulent flow near a wall, J. Aeronaut. Sci. 23 (1956) 1007–1011.
[33] W. Rodi, Experience with two-layer models: combining the k–ε model with a one-equation model near the wall, AIAA Paper 91-0216, 1990.
[34] T. Cebeci, P. Bradshaw, Physical and computational aspects of convective heat transfer, Springer-Verlag, New York, NY, 1984.
[35] H. Schlichting, Boundary Layer Theory, seventh ed., McGraw-Hill, New York, NY, 1979.
[36] R.L. Panton, Incompressible Flow, John Wiley and Sons, New York, NY, 1984.
[37] J.E. Dec, J.O. Keller, I. Hongo, Time-resolved velocities and turbulence in the oscillating flow of a pulse combustor tail pipe, Combust. Flame 83 (1991) 271–292.
[38] H.C. Chen, V.C. Patel, Near-wall turbulence models for complex flows including separation, AIAA J. 26 (1988) 641–648.
[39] W.C. Reynolds, Computation of turbulent flows, Ann. Rev. Fluid Mech. 8 (1975) 183–208.
[40] Z.M. Mao, T.J. Hanratty, Studies of the wall shear stress in a turbulent pulsating pipe flow, J. Fluid Mech. 170 (1986) 545–564.
[41] T. Cebeci, Behavior of turbulent flow near a porous wall with pressure, AIAA J. 8 (12) (1970) 2152.
[42] R.J. Moffat, W.M. Kays, A review of turbulent boundary layer heat transfer research at Stanford: 1958–1983, Adv. Heat Transfer 16 (1984) 241–365.
[43] J.E. Dec, J.O. Keller, V.S. Arpaci, Heat transfer enhancement in the oscillating turbulent flow of a pulse combustor tail pipe, Int. J. Heat Mass Transfer 35 (9) (1992) 2311–2325.